Tissue Damage by Pulsed Electrical Stimulation

A. Butterwick*, A. Vankov, P. Huie, Y. Freyvert, and D. Palanker

***Abstract*—Repeated pulsed electrical stimulation is used in a multitude of neural interfaces; damage resulting from such stimulation was studied as a function of pulse duration, electrode size, and number of pulses using a fluorescent assay on chick chorioallontoic membrane (CAM) *in vivo* and chick retina *in vitro*. Data from the chick model were verified by repeating some measurements on porcine retina *in-vitro*. The electrode size varied from 100 μm to 1 mm, pulse duration from 6 μs to 6 ms, and the number of pulses from 1 to 7500. The threshold current density for damage was independent of electrode size for diameters greater than 300 μm, and scaled as $1/r^2$ for electrodes smaller than 200 μm. Damage threshold decreased with the number of pulses, dropping by a factor of 14 on the CAM and 7 on the retina as the number of pulses increased from 1 to 50, and remained constant for a higher numbers of pulses. The damage threshold current density on large electrodes scaled with pulse duration as approximately $1/t^{0.5}$, characteristic of electroporation. The threshold current density for repeated exposure on the retina varied between 0.061 A/cm^2 at 6 ms to 1.3 A/cm^2 at 6 μs. The highest ratio of the damage threshold to the stimulation threshold in retinal ganglion cells occurred at pulse durations near chronaxie—around 1.3 ms.**

***Index Terms*—Electrical stimulation, electroporation, neural prosthesis, neural stimulation, retinal prosthesis.**

I. Introduction

AGE-RELATED macular degeneration (AMD) is the major cause of vision loss in people, who are more than 65 years of age in the Western world. As the average age of the population increases, the impact of AMD and other age-related retinal diseases becomes increasingly significant. Each year, 700 000 people are diagnosed with AMD, and 10% of these people become legally blind [1]. Retinitis pigmentosa (RP), the leading cause of inherited blindness, occurs in about one out of 4000 live births, which corresponds to approximately 1.5 million people worldwide [2]. In degenerative retinal diseases such as these, the photoreceptor layer of the retina degenerates, yet the inner retinal neurons, the "processing circuitry" downstream from the photoreceptors, are preserved at fairly high levels [3], [4]. Currently, there is no effective treatment for most patients with AMD or RP. However, if the inner retina could be stimulated appropriately, one might be able to bypass the function of the photoreceptors and restore some degree of sight.

Manuscript received January 20, 2006; revised March 5, 2007. This work was supported by the MFEL Grant from the Air Force Office of Scientific Research and NIH Grant 2R01 EY 012888. *Asterisk indicates corresponding author.*

*A. Butterwick is with the Department of Applied Physics, Stanford University, 445 Via Palou, Stanford, CA 94305 USA (e-mail: butterwick@stanford.edu).

A. Vankov, P. Huie, and D. Palanker are with the Department of Ophthalmology, Stanford University School of Medicine and with Hansen Experimental Physics Laboratory, Stanford University, Stanford, CA 94305 USA.

Y. Freyvert is with Sangamo BioSciences, Richmond, CA 94804 USA.

Color versions of one or more of the figures in this paper are available online at http://ieeexplore.ieee.org.

Digital Object Identifier 10.1109/TBME.2007.908310

Several groups, with different approaches, have proposed such designs for implants that would provide visual perception [5]–[7]. The most developed approach in the field stimulates retinal cells with an applied electric field. Acute and chronic electrical stimulation of the retina in patients with neurodegenerative diseases using arrays containing up to 16 electrodes has demonstrated the possibility of imparting perception of light, the detection of motion, and even simple shape discrimination [8], [9].

Electrical stimulation of neural cells is a powerful and broadly applicable therapeutic technology utilizing the voltage sensitivity of transmembrane ion channels and other fundamental processes of cellular electrical signaling. Therapies relying on electrical stimulation, such as deep brain stimulators, cochlear implants, or pacemakers often expose sensitive tissues to electric fields at supraphysiological levels. The concern for damage from chronic stimulation necessitates a detailed investigation of the damage thresholds. Several groups have investigated damage levels and mechanisms in various systems, including the cortex [10], heart [11], and to a much smaller degree, the retina [12], [13]. However, these studies have investigated only a very narrow set of parameters and have evaluated damage subjectively. A more thorough exploration of the scaling of the damage threshold with these parameters will help determine the optimal electrical stimulus for safe operation and perhaps elucidate the mechanisms of cellular damage.

The work of McCreery *et al.* (the publication most cited by the retinal prostheses community) established the current tenet in a series of experiments where the authors applied pulsed electric fields to the cat cortex *in vivo* with charge-balanced 400 μs pulses at 50 Hz over the course of 7 h [14]. In these experiments, tissue damage thresholds were defined in terms of current density and total injected current using electrodes of various sizes. Charge injection was fixed at 1 μC/phase, while the size of the electrode was varied in the first set of experiments. The authors determined the damage threshold charge density of 100 μC/cm^2 on an electrode size of 0.01 cm^2. In the second experiment, when the charge injection was varied on a fixed electrode size of 0.5 cm^2, damage was detected with a charge of 6 μC/phase and greater, corresponding to a threshold charge density of 12μC/cm^2. Since neither charge per phase nor charge density were conserved in these measurements, McCreery *et al.* concluded that the damage threshold is determined by an as yet-to-be-understood combination of the injected charge per phase and charge density. Shannon proposed an empirical model considering both charge density and charge per phase that was designed to agree with McCreery's data [15], but the manuscript contained little physical explanation to validate extrapolating the damage thresholds for arbitrary electrode sizes or levels of current injection. There has been even less investigation into the dependence of the damage threshold on pulse duration. This is in contrast to the strength-duration

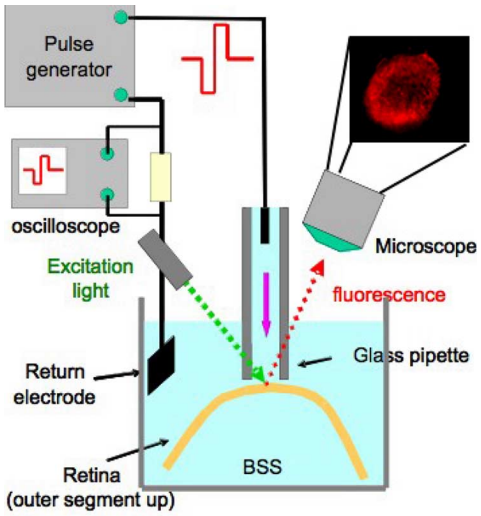

Fig. 1. Simplified diagram of the experimental setup (not to scale). The photograph insert demonstrates a typical appearance of the PI staining in the retina.

relationship of excitable cell stimulation, which has been well studied [16]–[20].

This study was motivated by the need for better understanding of the safe limits in acute and chronic electrical stimulation of biological tissue in general and retinal tissue in particular. We explore the dependence of the damage threshold on electrode size, pulse duration, and number of pulses using non-neural (chick chorioallontoic membrane *in vivo*) and neural (chick retina *in vitro*) tissue. In various experiments, damage thresholds were also determined in adult mammalian retina to ensure that the embryonic chick retinal model is appropriate.

II. Methods

Electrical stimulation was blanced-biphasic, with similar durations in both phases, and leading with the cathodal phase. All durations that will be mentioned refer to the pulse length per phase. Biphasic pulses were generated by a combination of two separate synchronized, monophasic voltage pulse generators. The output current was determined by measuring the voltage drop across a resistor connected between the return electrode in the medium and the ground electrode of the pulse generator, as shown in Fig. 1.

Tissue damage was assessed using a standard membrane permeability assay based on propidium iodide (PI) fluorescent dye (Sigma-Aldrich, St. Louis, MO) [21]–[23]. PI is a normally cell-impermeant molecule, which undergoes a 40-fold enhancement of fluorescence upon binding to nucleic acids. PI fluorescence of the cell indicates abnormal permeability of the cell membrane or even disintegration of the membrane and nucleus [24], [25]. Even though transient permeabilization of the cell membrane does not always lead to immediate cellular death, it is certainly of abnormal state and cannot be sustained chronically. For the assessment of fluorescence, the tissue was imaged through an emission filter (Chroma, Rockingham, VT) positioned in front of the objective lens of a stereomicroscope (Bausch & Lomb, Rochester, NY) with the excitation illumination provided by a fiber-coupled Xenon lamp (OTI, XE-Lite, Toronto, ON, Canada) through an excitation filter. PI was added to the medium prior to the treatment and fluorescence of the tissue was assessed 15 min. after completion of the electrical insult.

Cellular damage can result from the direct effects of the electric field (e.g., electroporation) as well from the toxic products of the electrochemical reactions at a metal-electrolyte interface. Platinum electrodes with a very large exposed surface area eliminated the possibility of any cellular toxicity from chemical byproducts of the electrical current. The large electrodes were placed in saline-filled glass pipettes with a much smaller aperture to minimize the injected current densities at the electrode electrolyte interface, and the electrical return was placed far away from the pipette tip, as illustrated in Fig. 1. Glass pipettes were heated with a laser and pulled to a determined size using a standard pipette puller (P-2000, Sutter Instruments, Novato, CA); pipette diameters ranged from 0.05 to 1 mm in diameter in this investigation. Due to the large size of the metal electrodes, inside and outside the pipette, compared to the pipette aperture, the electrochemical potential drop at the metal surfaces was negligible compared to the resistive voltage drop in front of the aperture. Therefore, the pulse of current reproduced the square shape of the voltage pulse input; dividing the voltage by the measured current determined the impedance of the pipette. Pipette impedance was measured before each experiment to ensure that the circuit was functional and the pipette tip was not blocked—a test especially important for smaller pipettes. The pipette was mounted on a 3-D micromanipulator to position the aperture against the surface of the tissue. Two stereoscopes oriented at different angles were used to monitor the orientation and location of the pipettes. Fluorescence was detected using a stereoscope directly above the sample, while the assessment of the distance and orientation of the pipette relative to the tissue surface was better observed with the second microscope oriented 60° to the surface of the tissue.

Chicken embryos (E15 to E19) were used for most of the measurements because a large amount of tissue was required for this multivariable study and chick embryos offer an effective and practical *in vivo* and *in vitro* model for such experiments. Additionally, this source does not require an extensive animal protocol during this period of development [26]. For *in vivo* measurements on chorioallantoic membranes (CAM), the top air-filled portion of the eggshell was cracked and removed. The shell membrane was then separated from the CAM and removed [26], and the CAM was subsequently covered with Dulbecco's phosphate-buffered saline (DPBS) without phenol red (Invitrogen). The pipette was brought into close proximity to the tissue, while the return electrode was placed in the medium at least 1 cm away from the pipette. All measurements were performed at room temperature.

For *in vitro* measurements on chicken retina, the eyes were removed immediately after decapitation, hemisected, and placed in the medium. The vitreous was removed from the eyecup, and an incision was made through the sclera and choroid. The sclera was then removed and the retina was placed in a Petri dish oriented with the photoreceptor side up-toward the pipette, as shown in Fig. 1. Porcine retinal preparations were performed 1 h after euthanasia and enucleation. The eye was hemisected with a scissor and placed into Hank's buffered salt solution (HBSS)

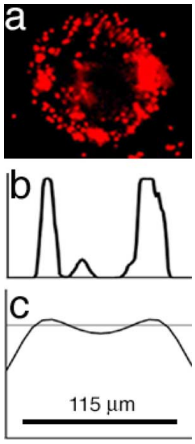

Fig. 2. (a) Example of typical damage pattern on CAM, as seen by PI fluorescence near the threshold current density levels. (b) Intensity histogram taken along the region highlighted in Fig. 2(a). This histogram corresponds to the distribution of an electric field from the pipette of 120 μm in diameter, shown in Fig. 2(c). The gray line in Fig. 2(c) represents an estimate of the damage threshold.

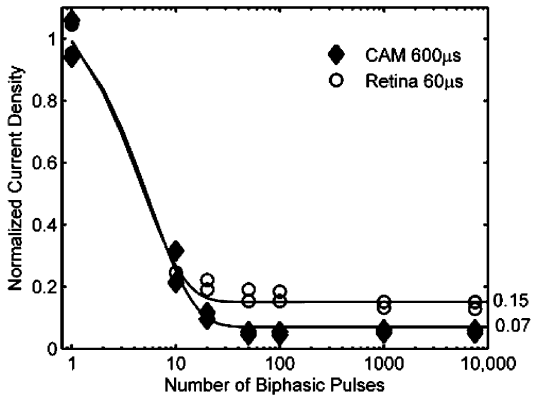

Fig. 3. Damage threshold current density for sustained repetitive stimulation on CAM and on retina, normalized to single exposure damage thresholds and plotted as a function of the number of pulses. After approximately 50 pulses in 5 min, the damage threshold reaches constant levels in both tissues. A pipette of 1 mm in diameter was used in these measurements with a pulse duration of 60 μs for CAM and 600 μs for the retina.

(invitrogen), where the vitreous, sclera, and choroid were immediately separated from the retina. Upon extraction, the retina was cut into 1-cm portions and placed photoreceptor-side up in a Petri dish.

Trials for the assessment of damaging current density levels on CAM and retina were taken for up to 2 h on each tissue preparation while samples were kept in HBSS at room temperature. During this period, the background fluorescence, measured in areas where tissues were not exposed to any electricity, remained low and the damage thresholds under identical settings remained constant. Every measurement was performed on an untreated region of the tissue. Tissue damage was determined by the appearance of a circular fluorescent pattern with its size similar to the pipette diameter and brightness exceeding the background level by at least a factor of two. Typically, the fluorescence of the damaged tissue increased a couple minutes after the treatment, but we allowed 15 min of delay for accurate determination near the threshold levels. Each data point was determined after five identical trials that consistently demonstrated either safe or damaging levels of stimulation.

III. Results

We applied pulsed stimulation to CAM *in vivo* and to the retinal preparations *in vitro* with pulse durations in the range of 6 μs/phase to 6 ms/phase, using tapered pipette electrodes with inner diameters ranging from 0.05 to 1 mm. Impedances for such pipettes ranged from 1.7–10.2 kΩ. For each setting, the current was increased until the fluorescent dye became detectable. The two points plotted in Figs. 3–6 for each pulse duration represent the maximum current density that reproducibly maintains PI exclusion from the cell and the minimum current density that reproducibly leads to the appearance of PI fluorescence. Images of typical damage patterns are shown in Figs. 1 and 2. At current densities near the damage threshold, the cells exhibit damage along the perimeter of the pipette while the tissue apposed to the interior region of the electrode is relatively unharmed. At higher current densities, when the electric field exceeds the damage threshold inside the circle, the whole disk exhibits a fluorescence that also extends beyond the boundaries of the pipette. The fluorescence image of a damaged region of CAM Fig. 2(a), is shown with a sectional histogram of image intensity [Fig. 2(b)]. Fig. 2(c) compares this to the distribution of the electric field from a pipette of diameter 120 μm [27]. Cross-sectional slices of PI-stained retina demonstrated that typically all three layers of nuclei (outer nuclear layer, inner nuclear layer, and ganglion cell layer) were fluorescent after damage.

The effect of the number of pulses on the damage threshold was investigated on both CAM *in vivo* and retina *in vitro*. To eliminate variability from the dynamics of PI uptake with the cells [28], the total exposure time was defined as 5 min and the number of pulses within that window was adjusted by varying the pulse repetition rate. Data in Fig. 3 represent the variation of the damage threshold with the number of pulses normalized to the damage threshold obtained with a single pulse. The damage threshold rapidly decreases with the number of pulses, reaching a stable minimum level as the number of pulses exceeds 50. These sustained thresholds in the retina and in CAM were approximately 7 and 14 times lower, respectively, than the single-pulse levels. Pulse durations in these measurements were 60 μs for CAM and 600 μs for the retina. A similar dependence was observed at other pulse durations (data not shown).

In the following tests, we defined the "regime of sustained repetitive pulsing" as 7500 pulses (25 Hz during 5 min). As shown graphically in Fig. 3, this pulse number exceeds the minimum (50) by more than two orders of magnitude. The chronic damage threshold might further decrease if exposure were extended to hours or even days. However, both the CAM *in vivo* and retinal *in vitro* preparations were found to survive for only a few hours. The techniques and models required for an experiment exploring a true chronic exposure would limit the investigation to only a small number of data points, similar to previous studies of this type [14]. By using an animal model that provides a fast and simple tissue preparation, convenient accessibility, and imaging of live tissue, a broad parameter space can be explored, though with limited exposure time.

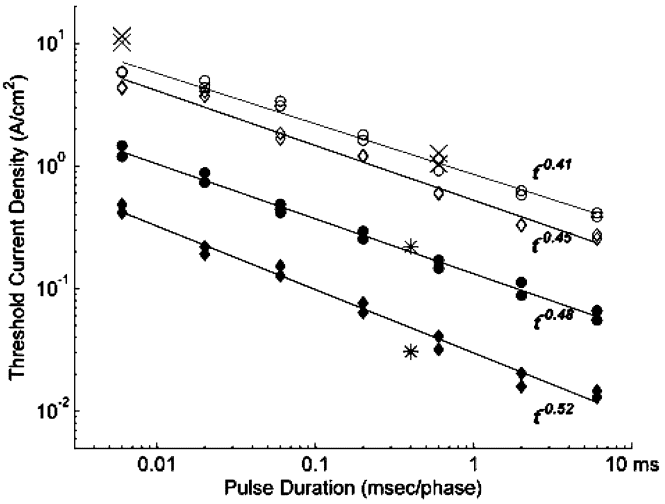

Fig. 4. Strength-duration dependence of the damage thresholds for chicken retina ($\circ$, $\bullet$) and CAM ($\diamond$, $\blacklozenge$), measured with single shots (open symbols) and with sustained repetitive exposures (solid symbols). Current density relates to pulse duration t roughly as $t^{-0.5}$, which is characteristic of electroporation [29], [30]. For comparison, the damage thresholds of the brain cortex by chronic stimulation *in-vivo* ($*$) [14] and of the porcine retina by single pulses *in-vitro* ($\times$) are presented on the same plot.

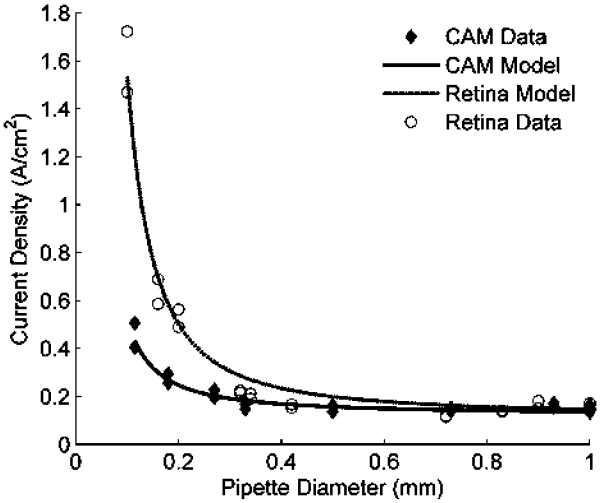

Fig. 5. Dependence of the threshold current density on pipette diameter for sustained exposures on retina and CAM. Solid and dashed lines represent the current density at the tissue, calculated using the model of a disk electrode located at the distances of 57 μm for CAM and 125 μm for retina. Pulse duration of 60 μs/phase was used for CAM and 600 μs/phase for the retina. In the regime of constant current, electrodes smaller than 200 μm, the threshold value of total current for damage is 139 μA on retina and 55 μA on CAM.

The strength-duration relationships for single-shot and for sustained repetitive exposures delivered to CAM *in-vivo* and to retina *in-vitro* with a pipette of 1-mm diameter are shown in Fig. 4. For comparison, we present, on the same plot, results from the previous study of chronic mammalian neural tissue exposure *in vivo* using similarly sized electrodes [14]. The data obtained with sustained exposuresare in good agreement with McCreery's chronic mammalian *in vivo* data [14], labeled with a star in Fig. 4. Both the single pulse and the sustained damage thresholds scale with pulse duration approximately as $1/\sqrt{t}$: the power fit slopes are $t^{-0.52}$ and $t^{-0.48}$ in the chronic regime, and $t^{-0.49}$ and $t^{-0.41}$ with the single shots on CAM and retina, respectively. Also shown are two data points taken on porcine retina *in vitro* in a manner similar to the measurements on the chicken retina. Porcine retina is a popular model in the retinal prosthesis community, and the good agreement of these results with the chicken retinal results supports the validity of the chicken embryo model for these measurements.

The effect of electrode size on the damage threshold during sustained repetitive stimulation is shown in Fig. 5. These measurements were performed with only one pulse of duration 60 μs on CAM and 600 μs on the retina. Different pulse durations were used for the two different tissues to yield similar damage thresholds on large electrodes (1 mm in diameter) for convenience of depiction on the same plot. The damage threshold current density is virtually independent of electrode size when electrodes larger than 0.3 mm are used. However, with smaller electrodes, the threshold current density increases with decreasing size; for very small electrodes, it scales with the reciprocal of the square of the pipette diameter. Therefore, small electrodes appear to act as a "point source," a regime in which the total current rather than current density determines the damage threshold. In this regime, for the plotted curves, the total current that causes damage on retina and CAM is 139 and 55 μA, respectively. The nature of the damage threshold dependence on electrode size will be further discussed.

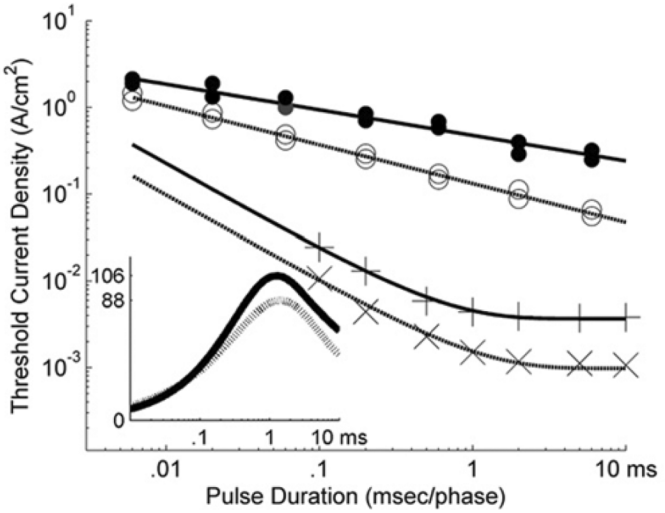

Fig. 6. Dependence of the chronic retinal damage threshold on pulse duration measured with pipettes of 0.12 ($\bullet$) and 1.0 mm ($\circ$) in diameter. For comparison, we plot stimulation thresholds of the retinal ganglion cells measured by Jensen *et al.* [16] using disk electrodes of similar sizes: 0.12 ($+$) and 0.5 ($\times$) mm in diameter. Ratios of the damage thresholds to the stimulation thresholds are shown in the insert for both electrodes.

The strength-duration dependences of the damage threshold, measured with pipettes of two different diameters—0.115 and 1.0 mm—are shown in Fig. 6.

Interestingly, not only are the absolute levels somewhat different, but the slopes are also $t^{-0.48}$ for the large pipette and $t^{-0.29}$ for the small one. For comparison, the plot also includes the strength-duration curves for stimulation thresholds measuring *in-vitro* on the rabbit retina using similar electrode diameters by Jensen *et al.* [16].

IV. Discussion

As shown in Fig. 4, the damage threshold current density j relates to the pulse duration t roughly as $j \propto t^{-0.5}$. Such scaling is characteristic for electroporation, a process in which nanometer-scale pores form in the lipid bilayer of a cell membrane under the pulsed electric field [29], [30]. Such scaling means that the charge density, $q = j \cdot t$, is not conserved along the strength-duration curve. This observation contradicts the earlier assumption that the charge and the charge density per phase are the only determinants of the damage threshold [14], [15]. The sustained level of the damage threshold for CAM in our experiments is very similar to that measured during chronic *in vivo* stimulation of the cat cortex using a large (0.5 cm^2) electrode [14]. The current density threshold for damage in retinal tissue appears to be three times higher than that for damage in CAM.

In addition to the direct effect of an electric field on a cellular membrane (electroporation), cellular damage can be caused by changes in pH, the toxic leaching of electrode materials into the electrolyte, or by cellular hyperthermia. To avoid formation of toxic byproducts on electrodes, platinum wire bundles with a very large surface area exposed to the electrolyte were inserted into the pipette electrodes. This design allowed surface current densities on the platinum wires to remain very low (well within the electrochemically safe range) while current densities at the aperture of the tapered pipette were much higher than a metal disk electrode of the same size would allow. Similar considerations were made for the large platinum return electrode.

Electric current produces Joule heat in the medium that, in principle, could lead to cellular hyperthermia and account for the damage seen. To assess the temperature changes in our experiments, we estimated the Joule heating from the electrode as follows. The time constant for heat diffusion across a distance L can be estimated as $\tau = L^2/(4k)$, where thermal conductivity k for water is 0.14 mm^2/s. Thus, thermal diffusion across a distance comparable to the electrode radius of 50 μm will take about 4.5 ms, while for 0.5 mm, it will take 0.45 s. Thus, for pulse durations and electrode sizes used in this study, the peak temperature after application of a single pulse can be estimated assuming the heat confinement conditions. On the other hand, the temperature rise during chronic stimulation can be estimated based on a steady-state temperature distribution achieved during infinitely long exposure.

The peak temperature reached after a single pulse can be estimated assuming that the current emanates from a spherical electrode equal in size to the pipette diameter. A temperature rise ΔT on a surface of a spherical electrode with radius r, by the end of a pulse with energy E, will be $\Delta T = E/(4\pi \cdot r^3 C \cdot \rho)$, where C and ρ are the heat capacity and density of water, respectively [31]. The energy E of a square pulse of current I of duration t is $E = I^2 \cdot R \cdot t$. Here, the resistance R of the medium between the spherical electrode of radius r and a large return electrode at infinity is $R = \gamma/(4\pi r)$, where γ is the resistivity of the medium (100 $\Omega \cdot$ cm in our case). Since on the surface of a spherical electrode the current density is $j = I/ \cdot 4\pi r^2$, the temperature rise ΔT can be rewritten as $\Delta T = j^2 \cdot t \cdot \gamma / c \cdot \rho$. If the damage threshold current density relates to pulse duration as $j \propto t^{-0.5}$, the peak temperature remains constant along the whole strength-duration curve. For a current density $j = 1\ \text{A}/\text{cm}^2$ and a pulse duration of $t = 1$ ms, $\Delta T = 17$ mK. Thus, no hyperthermia should be expected after the application of a single pulse at the damage threshold levels.

An upper estimate of the temperature rise ΔT on the surface of a spherical electrode during chronic stimulation can be obtained assuming that the heat is generated within a volume comparable to the size of the electrode and that the steady-state temperature distribution outside that sphere is determined by heat diffusion $\Delta T = P/(4\pi\lambda r)$, where P is the average power dissipated in the medium and $\lambda = 0.58 W/(m{\cdot}K)$ is the heat conductivity of water. For pulses applied at frequency ν, $P = I^2 {\cdot} R {\cdot} t {\cdot} \nu$ and, thus, $\Delta T = j^2 \cdot r^2 \cdot \gamma \cdot t \cdot \nu / \lambda$. For $r = 0.5$ mm, $\nu = 25$ Hz, $j = 0.17$ A/cm^2, and $t = 1$ ms, $\Delta T = 22$ mK. Therefore, no hyperthermia can be expected as a result of chronic stimulation with a repetition rate of 25 Hz at the current density corresponding to the sustained damage threshold levels observed in our experiments.

The measured dependence of the threshold current density on electrode size, shown in Fig. 5, can be predicted by calculating the current density j_{cell} at the target cell located at a distance z in front of the disk electrode which has a uniform current density j_0 on its surface $j_{\text{cell}}(z) = j_0(1 - z/\sqrt{r^2 + z^2})$. In other words, to produce a threshold current j_{cell} at distance z, the current density at the electrode should be $j_0(z) = j_{\text{cell}}(\sqrt{x^2+1}/\sqrt{x^2+1-1})$, where $x = r/z$.

This function best matches the experimental data for the retina with $z = 125$ μm, and for CAM with $z = 57$ μm, as plotted in Fig. 5. With the electrode much larger than the distance to the target tissue, $x \rightarrow \infty$ and $j_0 \approx j_{\text{cell}}$; the current density determines the damage threshold. As the pipette becomes smaller than the distance to the tissue, $x \rightarrow 0$, the current density scales quadratically with the distance z since $j_0 \approx j_{\text{cell}} \cdot 2z^2/r^2$, and the total current $I_0(z) = j_0 \cdot \pi \cdot r^2 \approx j_{\text{cell}} \cdot 2\pi z^2$ is conserved. This implies that a small electrode acts as a point source for the electric field and the total current rather than current density on the electrode determines the damage threshold. Although the disk model describes the general scaling of the damage threshold with distance and the size of the electrode rather well, this model is limited in its precision since it does not take into account variations of the tissue impedance and the enhancement of the electric field at the edges of the disk electrode. Fig. 2 shows the damage pattern observed when current densities are close to the threshold levels. In this case, only the enhanced electric field at the periphery exceeds the damage threshold, while the central part remains undamaged. For illustration, an estimated threshold of the cellular damage is shown with the horizontal line. When the current density was significantly larger than the threshold value, the damage pattern appeared as a solid disk.

Our principle motivation for studying the damage thresholds was to determine the safety limits for retinal prosthetics. Comparison of the damage levels to the neural stimulation thresholds determines the width of the safe therapeutic window for retinal stimulation. In Fig. 6, we compare the sustained retinal damage thresholds for two electrode sizes (0.12 and 1 mm in diameter) with data taken from the study by Jensen *et al.* on the stimulation thresholds of the rabbit retinal ganglion cells using similar electrode sizes (0.125 and 0.5 mm) [16]. Note that the damage thresholds were not determined in this study for the 0.5-mm

electrode size used by Jensen *et al.*, but the results summarized in Fig. 5 show little change in damage thresholds between the 0.5- and 1-mm diameter electrodes.

Comparing the damage and the stimulation thresholds allows for a determination of the optimal pulse duration at which the width of the safe therapeutic window is the largest. The ratio of the damage threshold, approximated as $j \propto A + B \cdot t^{-0.5}$, to the stimulation threshold, approximated as $j \propto R/(1-\exp(-t/\tau))$ [32], is plotted in an insert on Fig. 6. These ratios reach their maxima, 88 and 106, at pulse durations of 1.4 ms and 1.3 ms for 1.0-mm and 0.12-mm pipettes, respectively. A dynamic range of 100 is sufficiently broad to cover the linear response range of the neural cells (typically in the range of 10–30 [33], [34]) and, thus, is quite adequate for the purpose of prosthetic vision. It is important to note that although the damage and the stimulation thresholds are dependent on electrode size, their ratio, which determines the dynamic range of safe stimulation, appears to be practically size independent. Interestingly, recent measurements *in vivo* of the stimulation threshold in humans (electrode size 0.4 mm, $t = 1$ ms, $j = 0.01$ A/cm^2) [35] and the damage threshold in rabbits (electrode size 0.4 mm, $t = 1$ ms, $j = 0.46$ A/cm^2) [13] result in a just slightly lower ratio, 46.

V. Conclusion

This study determines regimes of safe electrical stimulation depending on the electrode size, pulse duration, and number of pulses. For electrodes of diameters larger than the distance to the target cells, the current density determines the damage. For small electrodes (diameters less than 200 μm in our experiments), which act as point sources, the total current determines the damage threshold. Threshold current density scales with pulse duration approximately as $1/\sqrt{t}$. This implies that the charge is not conserved along the strength-duration curve, and that the width of the safe therapeutic window (i.e., the ratio of damage threshold to stimulation threshold) depends on pulse duration.

Acknowledgment

The authors would like to thank I. Hakim, E. Anderson, and N. Palanker for technical help in many aspects of the experimental protocol, and R. Jensen, who kindly provided his experimental data on retinal stimulation for comparison.

References

[1] C. A. Curcio, N. E. Medeiros, and C. L. Millican, "Photoreceptor loss in age-related macular degeneration," *Invest. Ophthal. Vis. Sci.*, vol. 37, no. 7, pp. 1236–49, 1996.

[2] E. L. Berson, B. Rosner, M. A. Sandberg, K. C. Hayes, and B. W. Nicholson, "Vitamin A supplementation for retinitis pigmentosa," *Arch Ophthal.*, vol. 111, no. 11, pp. 1456–9, 1993.

[3] A. Santos, M. S. Humayun, E. de Juan, Jr., and R. J. Greenberg, "Preservation of the inner retina in retinitis pigmentosa a morphometric analysis," *Archives Ophthal.*, vol. 115, no. 4, pp. 511–5, 1997.

[4] J. L. Stone, W. E. Barlow, M. S. Humayun, E. de Juan, Jr., and A. H. Milam, "Morphometric analysis of macular photoreceptors and ganglion cells in retinas with retinitis pigmentosa," *Archives Ophthal.*, vol. 110, no. 11, pp. 1634–1639, 1992.

[5] J. Wyatt and J. Rizzo, "Ocular implants for the blind," *IEEE Spectr.*, vol. 33, no. 5, pp. 47–47, May 1996.

[6] W. Liu, E. McGuken, M. Clemments, K. Vichienchom, C. Demarco, M. S. Humayun, E. de Juan, J. Weiland, and R. Greenberg, "The engineering of a prototype retinal prosthesis," *Invest. Ophthal. Vis. Sci.*, vol. 40, no. 4, pp. S782–S782, 1999.

[7] R. A. Normann, E. M. Maynard, P. J. Rousche, and D. J. Warren, "A neural interface for a cortical vision prosthesis," *Vis. Res.*, vol. 39, no. 15, pp. 2577–87, 1999.

[8] M. Humayun, R. J. Greenberg, B. V. Mech, D. Yanai, M. Mahadevappa, G. van Boemel, G. Y. Fujii, J. D. Weiland, and E. de Juan, "Chronically implanted intraocular retinal prosthesis in two blind subjects," *Invest. Ophthal. Vis. Sci.*, vol. 44, pp. U467–U467, 2003.

[9] M. S. Humayun, E. de Juan, G. Dagnelie, R. J. Greenberg, R. H. Prost, and D. H. Phillips, "Visual perception elicited by electrical stimulation of retina in blind humans," *Archives Ophthal.*, vol. 114, no. 1, pp. 40–46, 1996.

[10] H. Asanuma and A. P. Arnold, "Noxious effects of excessive currents used for intracortical microstimulation," *Brain Res.*, vol. 96, no. 1, pp. 103–7, 1975.

[11] A. T. Sambelashvili, V. P. Nikolski, and I. R. Efimov, "Virtual electrode theory explains pacing threshold increase caused by cardiac tissue damage," *Amer. J. Phys. Heart Circ. Physiol.*, vol. 286, no. 6, pp. H2183–94, 2004.

[12] F. Gekeler, K. Kobuch, H. N. Schwahn, A. Stett, K. Shinoda, and E. Zrenner, "Subretinal electrical stimulation of the rabbit retina with acutely implanted electrode arrays," *Graefes Archive Clin. Exper. Ophthal.*, vol. 242, no. 7, pp. 587–596, 2004.

[13] Y. Yamauchi, V. Enzmann, L. M. Franco, D. Jackson, J. F. Naber, I. Rizzo, J. F. Ziv, R. O. Ziv, and H. J. Kaplan, "Subretinal placement of the microelectrode array is associated with a low threshold for electrical stimulation," presented at the Annu. Meeting Assoc. Res. Vision Ophthalmology, Fort Lauderdale, FL, 2005.

[14] D. B. McCreery, W. F. Agnew, T. G. Yuen, and L. Bullara, "Charge density and charge per phase as cofactors in neural injury induced by electrical stimulation," *IEEE Trans. Biomed. Eng.*, vol. 37, no. 10, pp. 996–1001, Oct. 1990.

[15] R. V. Shannon, "A model of safe levels for electrical stimulation," *IEEE Trans. Biomed. Eng.*, vol. 39, no. 4, pp. 424–6, Apr. 1992.

[16] R. J. Jensen, J. F. Rizzo, 3rd, O. R. Ziv, A. Grumet, and J. Wyatt, "Thresholds for activation of rabbit retinal ganglion cells with an ultrafine, extracellular microelectrode," *Invest. Ophthal. Vis. Sci.*, vol. 44, no. 8, pp. 3533–3543, 2003.

[17] R. J. Jensen, O. R. Ziv, and J. F. Rizzo 3rd, "Thresholds for activation of rabbit retinal ganglion cells with relatively large, extracellular microelectrodes," *Invest. Ophthal. Vis. Sci.*, vol. 46, no. 4, pp. 1486–1496, 2005.

[18] B. J. Roth, "A mathematical-model of make and break electrical-stimulation of cardiac tissue by a unipolar anode or cathode," *IEEE Trans. Biomed. Eng.*, vol. 42, no. 12, pp. 1174–1184, Dec. 1995.

[19] B. J. Roth, "Mechanisms for electrical-stimulation of excitable tissue," *Crit. Rev. Biomed. Eng.*, vol. 22, no. 3-4, pp. 253–305, 1994.

[20] I. Mogyoros, M. C. Kiernan, and D. Burke, "Strength-duration properties of human peripheral nerve," *Brain*, vol. 119, pp. 439–447, 1996.

[21] M. O. Bevensee, C. J. Schwiening, and W. F. Boron, "Use of BCECF and propidium iodide to assess membrane integrity of acutely isolated CA1 neurons from rat hippocampus," *J. Neurosci. Methods*, vol. 58, no. 1-2, pp. 61–75, 1995.

[22] F. Belloc, P. Dumain, M. R. Boisseau, C. Jalloustre, J. Reiffers, P. Bernard, and F. Lacombe, "A flow cytometric method using Hoechst 33342 and propidium iodide for simultaneous cell cycle analysis and apoptosis determination in unfixed cells," *Cytom.*, vol. 17, no. 1, pp. 59–65, 1994.

[23] G. J. Wilde, L. E. Sundstrom, and F. Iannotti, "Propidium iodide in vivo: An early marker of neuronal damage in rat hippocampus," *Neurosci. Lett.*, vol. 180, no. 2, pp. 223–6, 1994.

[24] C. J. Yeh, B. L. Hsi, and W. P. Faulk, "Propidium iodide as a nuclear marker in immunofluorescence. II. Use with cellular identification and viability studies," *J. Immunol Methods*, vol. 43, no. 3, pp. 269–75, 1981.

[25] I. U. Cevik and T. Dalkara, "Intravenously administered propidium iodide labels necrotic cells in the intact mouse brain after injury," *Cell Death Different.*, vol. 10, pp. 928–929, 2003.

[26] T. Leng, J. M. Miller, K. V. Bilbao, D. V. Palanker, and P. Huie, "The chick chorioallantoic membrane as a model tissue for surgical retinal research and simulation," *Retina-J. Retinal Vitr. Diseases*, vol. 24, no. 3, pp. 427–434, 2004.

[27] A. M. Mierisch, S. R. Taylor, and V. Celli, "Understanding the degradation of organic coatings through local electrochemical impedance methods—II. Modeling and experimental results of normal field variations above disk electrodes," *J. Electrochem. Soc.*, vol. 150, no. 7, pp. B309–B315, 2003.
[28] J. D. Deng, K. H. Schoenbach, E. S. Buescher, P. S. Hair, P. M. Fox, and S. J. Beebe, "The effects of intense submicrosecond electrical pulses on cells," *Biophys. J.*, vol. 84, no. 4, pp. 2709–2714, 2003.
[29] E. Neumann, "Membrane electroporation and direct gene-transfer," *Bioelectrochem. Bioenergetics*, vol. 28, no. 1-2, pp. 247–267, 1992.
[30] E. Neumann, K. Tonsing, and P. Siemens, "Perspectives for microelectrode arrays for biosensing and membrane electroporation," *Bioelectrochem.*, vol. 51, no. 2, pp. 125–32, 2000.
[31] D. Palanker, I. Turovets, and A. Lewis, "Electrical alternative to pulsed fiber-delivered lasers in microsurgery," *J. Appl. Phys.*, vol. 81, no. 11, pp. 7673–7680, 1997.
[32] J. Malmivuo and R. Plonsey, *Bioelectromagnetism: Principles and Applications of Bioelectric and Biomagnetic Fields*. New York: Oxford Univ. Press, 1995, pp. 482–482.
[33] X. L. Yang and S. M. Wu, "Response sensitivity and voltage gain of the rod- and cone-bipolar cell synapses in dark-adapted tiger salamander retina," *J. Neurophysiol.*, vol. 78, no. 5, pp. 2662–73, 1997.
[34] A. Berntson and W. R. Taylor, "Response characteristics and receptive field widths of on-bipolar cells in the mouse retina," *J. Physiol.*, vol. 524, pt. 3, pp. 879–89, 2000.
[35] M. Mahadevappa, J. D. Weiland, R. J. Greenberg, and M. S. Humayun, "Perceptual thresholds and electrode impedance in three retinal prosthesis subjects," *IEEE Trans. Neural Syst. Rehab. Eng.*, vol. 13, no. 2, pp. 201–206, Jun. 2005.

A. Butterwick received the B.S.E. degree in engineering physics from the University of Michigan, Ann Arbor, in 2002 and the M.S. degree in applied physics from Stanford University, Stanford, CA, in 2005, where he is currently pursuing the Ph.D. degree in applied physics.

Currently, he is interested in understanding the interactions between electric fields and tissues toward developing novel therapies.

A. Vankov, photograph and biography not available at time of publication.

P. Huie, photograph and biography not available at time of publication.

Y. Freyvert was born in St. Petersburg, Russia, on August 23, 1986.

He was a Volunteer at the San Francisco Veterans Hospital and a Research Assistant in the Department of Ophthalmology, Stanford University, and a Research Apprentice in the Department of Education for the University of California, Berkeley. Currently, he is an Intern with Sangamo BioSciences, Richmond, CA.

D. Palanker received the M.S. degree in physics from the Armenian State University, Yerevan, Russia, in 1984, and the Ph.D. degree in applied physics (biomedical optics) from the Hebrew University of Jerusalem, Israel, in 1994.

Currently, he is an Associate Professor in the Department of Ophthalmology, School of Medicine, and Hansen Experimental Physics Laboratory, Stanford University, Stanford, CA. His research focuses on the interactions of electric field and light with biological cells and tissues, and applications of these interactions to diagnostic, therapeutic, and prosthetic technologies. He has authored more than 70 scientific publications and two book chapters in the field of biomedical optics and electronics, and has received 11 U.S. and international patents.